



Plasma Graft Copolymerization of 4-Vinylpyridine on Dense and Porous SiLK for Electroless Plating of Copper and for Retardation of Copper Diffusion

Y. Q. Zhu,^a E. T. Kang,^{a,z} K. G. Neoh,^a T. Osipowicz,^b and L. Chan^c

^aDepartment of Chemical Engineering, National University of Singapore, Singapore 119260

^bDepartment of Physics, National University of Singapore, Singapore 117542

^cChartered Semiconductor Manufacturing, Limited, Singapore 738406

Argon plasma-pretreated dense and porous SiLK films coated on Si(100) wafers (Si-SiLK wafers) were subjected to plasma graft polymerization of 4-vinylpyridine (4VP). X-ray photoelectron spectroscopy and Fourier transform infrared spectroscopy results revealed that the pyridine functional groups of the plasma graft-polymerized 4VP (pp4VP) could be retained to a large extent under certain glow discharge conditions. The topography of the pp4VP grafted Si-SiLK (Si-SiLK-g-pp4VP) surface was studied by atomic force microscopy. The preserved pyridine groups were used as the chemisorption sites for the palladium complexes (without prior sensitization by SnCl₂) to catalyze the electroless deposition of copper. Rutherford backscattering spectrometry and transmission electron microscopy were employed to investigate the extent of copper diffusion into the pristine and graft-modified Si-SiLK substrates after thermal annealing. The grafted pp4VP layer on the dense and porous Si-SiLK surface served effectively as (i) a sensitization layer for the electroless plating of copper, (ii) an adhesion promotion layer for the electrolessly deposited copper, and (iii) a diffusion barrier for the electrolessly deposited copper. These functionalities arose from strong interactions of the metal ions and atoms with the pyridine moieties of the grafted pp4VP layer.

© 2005 The Electrochemical Society. [DOI: 10.1149/1.1952767] All rights reserved.

Manuscript submitted December 15, 2004; revised manuscript received March 25, 2005. Available electronically July 21, 2005.

The phenomenon of metal diffusion in polymers has important technological implications in microelectronics. The cross-talk noise and resistance-capacitance signal delay are fast becoming limiting factors in ultralarge scale integration (ULSI).¹ To address these problems, the conventional aluminum and SiO₂, which made up the multilayer metallization structure at the chip level, are being replaced by copper and polymers of low dielectric constants, such as polyimides.²⁻⁴ The dielectric constants of polymers can be further reduced through the introduction of a porous structure.^{5,6} One of the major drawbacks for copper is its high diffusivity in silicon, resulting in deterioration of the devices even at low temperatures.⁷ Moreover, copper has very poor adhesion with pristine polymers, and exhibits high diffusivity in polymers, especially at elevated temperatures.^{8,9} Diffusion barriers for minimizing copper diffusion into polymers are thus of interest.¹⁰ Accordingly, problems related to film stress, surface roughness, and interfacial properties of the barrier have to be resolved.

Various copper metallization techniques, such as physical vapor deposition (PVD), electroplating (EP), sputtering, and electroless plating (ELP) have been developed.^{11,12} Among them, electroless plating is of increasing interest due to its low cost, low processing temperature, and the ease of implementation.¹³ The conventional process for electroless plating of copper involves surface sensitizing by acidic SnCl₂, surface activation in PdCl₂ solution, and finally copper metallization.¹⁴⁻¹⁶ It has also been reported that the palladium ions can be adsorbed directly onto the pyridine groups of the self-assembled silane monolayers.¹⁷ The low-dielectric-constant (low- κ) polymer, SiLK,¹⁸⁻²⁰ developed by Dow Chemical Company, is a promising material with a low dielectric constant of 2.65 and good thermal stability.²¹ With the introduction of porous structure, the dielectric constant can be reduced to below 2.2. However, direct metallization of copper on pristine SiLK is difficult. The surface inertness of the SiLK polymer dictates the need for surface modification prior to copper metallization. Surface modification of polymers by graft copolymerization of functional monomers has been found to be an effective method for improving the adhesion of copper to polymers, such as poly(tetrafluoroethylene)²²⁻²⁴ and polyimides.²⁵

In this work, surface modification of dense and porous SiLK on Si(100) surfaces (Si-SiLK surfaces) via plasma polymerization of

4-vinylpyridine (4VP) was carried out. The chemical composition and topography of the Si-SiLK surface with plasma graft-copolymerization 4VP (Si-SiLK-g-pp4VP surface) were characterized by X-ray photoelectron spectroscopy (XPS) and atomic force microscopy (AFM), respectively. The adhesion strength of copper to the Si-SiLK-g-pp4VP surface was evaluated by the 180°-peel adhesion strength measurements. For diffusion studies, copper seed layers were electrolessly deposited onto the Si-SiLK and Si-SiLK-g-pp4VP surfaces, followed by annealing at 300°C for 5 h under vacuum. The extent of copper diffusion was revealed by Rutherford backscattering spectrometry (RBS). The RBS data were further supported by transmission electron microscope (TEM) imaging of the SiLK-metal interface.

Experimental

Materials.—The dense Si(100)-SiLK substrates (SiLK thickness = 0.8 μm , as measured by ellipsometry) were processed by Chartered Semiconductor Manufacturing Co., Ltd., Singapore. The porous Si(100)-SiLK substrates (SiLK thickness = 0.6 μm , as determined from the scanning electron microscopy cross-sectional images) were obtained from Institute of Microelectronics, Singapore. The SiLK surface was cleaned with absolute ethanol and dried under reduced pressure. The monomer, 4VP, was obtained from Aldrich Chemical Co. of Milwaukee, WI, and was further purified by vacuum distillation.

Plasma graft polymerization of 4VP on Si-SiLK surface: The Si-SiLK-g-pp4VP.—The plasma polymerization system was manufactured by Samco International of Kyoto, Japan (model Samco BP-1). The physical geometry of the system had been described in detail previously.²⁶ The radio frequency (rf) generator provided power supplies varying from 0 to 200 W and was operated at a frequency of 13.56 MHz. The plasma deposition process was performed between two circular parallel-plate electrodes of 10 cm in diameter in a Pyrex bell-jar chamber of about 6000 cm³ in volume. The Si-SiLK samples were placed on the ground electrode, which was about 2.8 cm away from the biased electrode. The samples were preactivated by the argon plasma at a fixed argon flow rate of 20 sccm for 5 s under a constant system pressure of 100 Pa. The power was varied between 5 and 70 W. After surface activation, the 4VP monomer at a specific temperature (4°C) was introduced into the deposition chamber by the argon carrier gas flowing through the thermostated monomer reservoir. All the gas lines were completely insulated. The monomer-carrier gas mixture was allowed to flow

^z E-mail: cheket@nus.edu.sg

evenly into the reactor chamber from a distributor located in the upper electrode. In all cases, the carrier gas stream was assumed to be saturated with the 4VP monomer, as dictated by the partial pressure of the latter. The system pressure was varied between 60 and 200 Pa. The gas flow rate was varied from 10 to 50 sccm. After impedance matching, the glow discharge was ignited. The plasma-polymerized 4VP (pp4VP) samples were obtained after a fixed deposition time of 45 s (for the Si-SiLK surface) or 4 min (for the KBr pellet surface, see below). The 4VP plasma graft-polymerized Si-SiLK surface was referred to as the Si-SiLK-g-pp4VP surface. Each Si-SiLK-g-pp4VP sample was immersed in a large volume of ethanol at 37°C with continuous stirring for at least 4 h to remove the residual amount of the physically adsorbed 4VP monomer, oligomer, and homopolymer.

Characterization of the pp4VP films and the Si-SiLK-g-pp4VP surfaces.—The chemical composition of the pristine and Si-SiLK-g-pp4VP surfaces was determined by XPS. The XPS measurements were performed on a Kratos AXIS HSi spectrometer using the monochromatized Al K α X-ray source (1486.71 eV photons) with a pass energy of 40 eV. The samples were mounted on the sample studs by means of double-sided adhesive tapes. The XPS signals were obtained at a photoelectron take-off angle (with respect to the sample surface) of 90°. The X-ray source was run at a power of 150 W (15 kV and 10 mA). The pressure in the analysis chamber was maintained at 10⁻⁸ Torr or lower during each measurement. All binding energies (BEs) were referenced to the C 1s hydrocarbon peak at 284.6 eV. Surface elemental stoichiometries were determined from XPS spectral area ratios, after correcting with the experimentally determined sensitivity factors. The sensitivity factors were calibrated using stable binary compounds of well-established stoichiometries.

The pp4VP samples for Fourier transform infrared (FTIR) spectroscopy measurements were obtained by direct deposition of the plasma-polymerized pp4VP films on freshly pressed KBr disks. Each FTIR spectrum was collected by cumulating 16 scans at a resolution of 8 cm⁻¹. All spectra were recorded under ambient conditions on a Bio-Rad FTIR, model 400, spectrophotometer. The pp4VP films were also deposited on pristine Si(100) wafers, which were transparent to infrared in the wavelength region of interest, for comparison purposes. No substrate dependence of the FTIR spectra of pp4VP films was discernible.

The surface topography of the pristine SiLK, Ar plasma-pretreated SiLK, and Si-SiLK-g-pp4VP samples was studied on a Nanoscope IIIa atomic force microscope from Digital Instruments, Inc. In each case, an area of 5 × 5 μm was scanned using the tapping mode. The drive frequency was 330 ± 50 kHz, and the voltage was between 3.0 and 4.0 V. The drive amplitude was about 300 mV and the scan rate was between 0.5 and 1.0 Hz. The arithmetic mean of the surface roughness (R_a) was calculated from the roughness profile.

Electroless plating of copper on the Si-SiLK-g-pp4VP surface and the adhesion strength measurement.—The Si-SiLK-g-pp4VP surfaces were activated through the immobilization of a palladium catalyst for the subsequent electroless plating of copper. For the Sn-free process, the Si-SiLK-g-pp4VP surface was exposed directly to an aqueous solution containing 0.1 wt % PdCl₂ and 1.0 wt % HCl (12 M) for 10 min, followed by rinsing with copious amounts of doubly distilled water. The surface-activated Si-SiLK-g-pp4VP substrate was then immersed in an electroless copper plating bath for 10 min. The composition of the copper plating bath was as follows: 10 g/L of copper sulfate pentahydrate (CuSO₄·5H₂O), 50 g/L of potassium sodium tartrate [KOCO(CHOH)₂COONa], 10 g/L of sodium hydroxide (NaOH), and 9.5 g/L of formaldehyde (CH₃CHO).²⁷ A copper layer of about 180 nm in thickness (estimated from SEM cross-sectional view) was deposited. The copper-metallized Si-SiLK-g-pp4VP surface was then rinsed thoroughly with copious amounts of doubly distilled water.

A copper sheet backing (0.1 mm in thickness) was adhered to the deposited copper surface using an epoxide adhesive [Araldite Standard, from Ciba Specialty Chemicals (UK), Duxford, England] for the subsequent 180°-peel adhesion strength measurements. The assemblies were thermally cured in a vacuum oven at 100°C for 3 h prior to the 180°-peel adhesion test. The 180°-peel adhesion strength was measured at room temperature on an Instron 5544 tensile tester. All measurements were carried out at a cross-head speed of 10 mm/min. For each adhesion strength reported, at least three sample measurements with variation within ±0.3 N/cm were averaged.

For comparison purposes, electroless metallization of the pristine SiLK and Si-SiLK-g-pp4VP surfaces was also carried out via the conventional two-step process.²⁷ In this method, the surfaces were first sensitized in an aqueous solution containing 3 wt % SnCl₂ and 2.5 wt % HCl (12 M) for 2 min, followed by rinsing with doubly distilled water. The subsequent activation in PdCl₂ solution, electroless plating of copper, attachment of the copper sheet backing, post-thermal treatment, and the adhesion strength measurements were similar to those described above.

Copper diffusion study by RBS and TEM.—The samples for copper diffusion studies were processed as follows. The surface-activated (Pd-laden) samples were immersed into the copper plating bath for only 90 s to deposit a thin copper seed layer. Scanning electron microscopy (SEM) images were used to ensure that the samples were covered with a uniform and thin copper seed layer. These samples were then annealed under vacuum for 5 h at 300°C. After annealing, further electroless deposition of copper to a thickness of ~100 nm was carried out. The second metallization process was mainly to provide a sizeable copper peak in the RBS spectrum so as to facilitate the comparison of the copper diffusion profiles. RBS of 2 MeV He⁺ was used to analyze the depth profiles of copper before and after annealing.

To show the extent of copper diffusion into the polymer matrix, TEM images of the cross section were obtained. The cross-sectional TEM investigation was carried out using a JEOL TEM (JEM-2010) with the electron-beam operated at an acceleration voltage of 200 kV. The cross-sectional sample preparation technique involves four main steps, viz., cutting, polishing, grinding, and ion milling. Two small pieces of the copper-metallized Si-SiLK-g-pp4VP substrates or Si-SiLK-g-pp4VP-Cu substrates, 2 × 4 mm in area, were first glued together face to face (copper to copper). Mechanical polishing and grinding were used to polish the cross section of the adhered samples. After that, the cross-sectional surface of the sample was ion-milled using two ion guns until the sample was transparent to electrons.

Results and Discussion

The processes of Ar plasma pretreatment of the pristine Si-SiLK surface, plasma graft polymerization of 4VP on the Si-SiLK surface to give rise to the Si-SiLK-g-pp4VP surface, surface activation by PdCl₂ in the absence of prior sensitization by SnCl₂, and electroless plating of copper are shown schematically in Fig. 1. The details of each process are discussed below.

Effect of Ar plasma treatment on the composition of the SiLK surface.—Figure 2 shows the C 1s core-level and wide scan spectra of the pristine Si-SiLK surface (part a) and the Si-SiLK surface after 5 s of Ar plasma treatment at the rf power of 5 W (part b) and 70 W (part c), followed by air exposure. The C 1s core-level spectrum of the pristine SiLK film can be curved-fitted with three peak components with BEs at 284.6, 286.2, and 291.2 eV, attributed to the C-H species, the C-O species, and the π-π* shake-up satellite, respectively.²⁸ Modification of the SiLK surface by Ar plasma, followed by air exposure, has resulted in the enhancement of the C-O peak component intensity. Two new peak components, with BEs at 287.6 and 289.2 eV, attributable to the C=O and O=C-O species,²⁸ respectively, are also discernible. Thus, the Ar

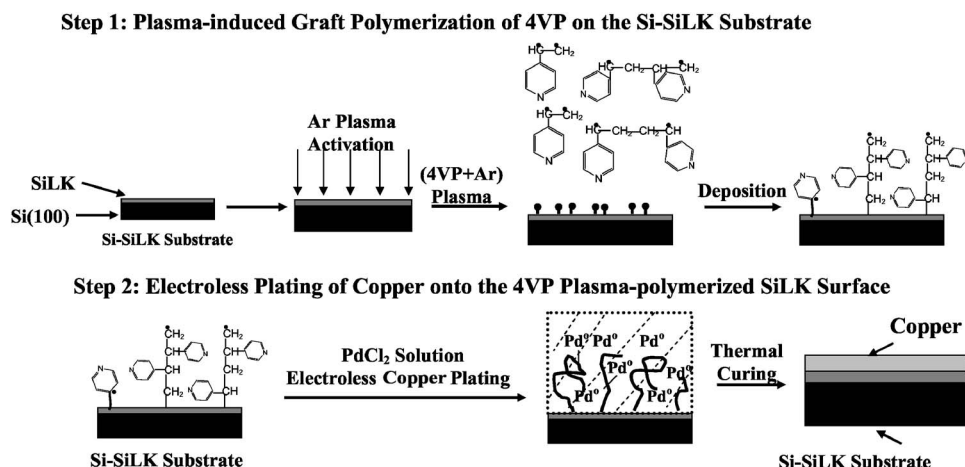


Figure 1. Schematic diagram illustrating the process of Ar plasma pretreatment, plasma graft polymerization, and copper metallization by electroless plating.

plasma activation process involves the formation of reactive species on the SiLK surface which are capable of reaction with oxygen upon exposure to air. The extent of plasma preactivation can, therefore, be assessed from the extent of surface oxidation for the sample after exposure to air. The reduction in intensity of the peak components associated with the π - π^* shake-up, carbonyl group, and carboxylic group in the C 1s spectrum of the 70 W argon plasma-pretreated sample suggests the onset of etching effect of the activated species at the high rf power. No aluminum signal is discernible in the wide scan spectrum of the argon plasma-pretreated SiLK surface. Thus, the SiLK surfaces are not contaminated by the electrode material of the glow discharge system.

Figure 3 shows the effect of Ar plasma rf power on the [O]/[C] ratio of the Si-SiLK surface after air exposure. For the plasma system used in this work and at a fixed pretreatment time of 5 s, the

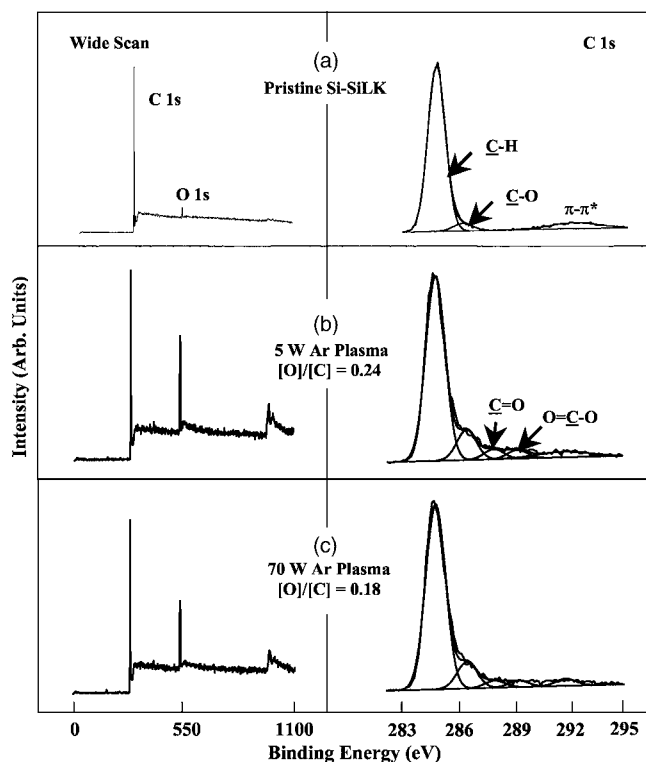


Figure 2. C 1s core-level and wide scan spectra of (a) the pristine Si-SiLK surface, and the 5 s Ar-plasma-pretreated SiLK surface at the rf power of (b) 5 and (c) 70 W, followed by air exposure.

[O]/[C] ratio decreases gradually, from the maximum value of 0.24 at 5 W, with the plasma rf power. The reduction in the [O]/[C] ratio is probably associated with the onset of the etching effect of the argon plasma on the surface-activated species under a higher rf power. Hence, the condition of Ar plasma preactivation was set at 5 W for 5 s in this study in order to minimize the etching effect.

Chemical structure of plasma-polymerized 4VP polymer.—The chemical structure of pp4VP was investigated first by FTIR spectroscopy. Figure 4 shows the respective FTIR spectra of the 4VP homopolymer (Fig. 4a) and of the pp4VP on KBr disks deposited at rf powers of 5 W (Fig. 4b) and 70 W (Fig. 4c). The FTIR spectrum of the 4VP homopolymer displays strong bending and stretching vibrations associated with the pyridine ring at 1416 and 1598 cm^{-1} , respectively.²⁹ The pp4VP films display the same characteristic adsorption bands of the 4VP homopolymer. However, for the pp4VP film deposited at the higher input rf power of 70 W, the C-H stretching absorption at 2968 cm^{-1} is enhanced. The appearance of this absorption band suggests that free methyl groups are formed in the plasma polymerization process and are incorporated into the pp4VP film. In addition, absorption bands at 2171 and 2217 cm^{-1} , attributable to the -N=C=N and -C=N structures, respectively,³⁰ are also discernible. The appearance of these vibration modes indicates the occurrence of pyridine ring-opening reaction under high plasma power.

Plasma polymerization differs significantly from the conventional ionic or radical polymerization. The process of plasma polymerization includes the fragmentation of monomer molecules, the

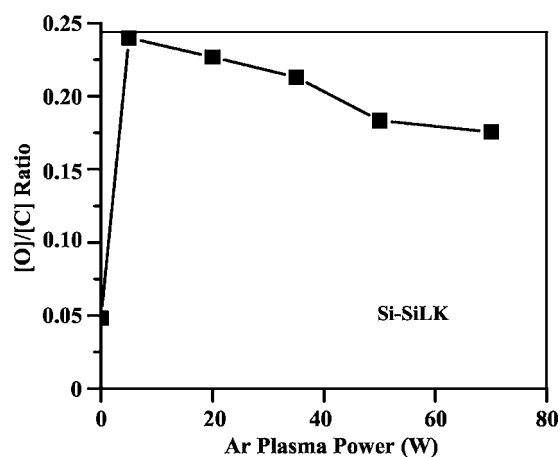


Figure 3. The dependence of [O]/[C] ratio of the Si-SiLK surface on the rf power (Ar plasma pretreatment time 5 s).

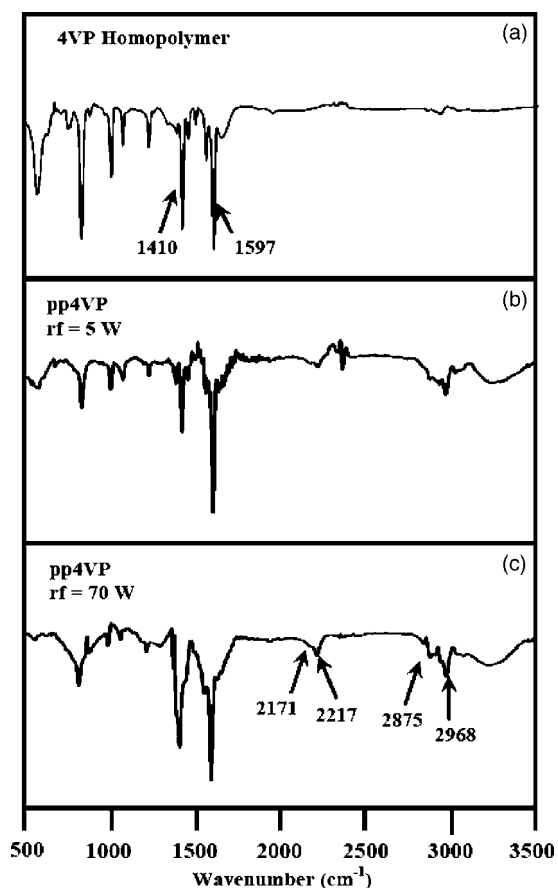


Figure 4. FTIR spectra of (a) the 4VP homopolymer, the pp4VP films on KBr pellets deposited at the rf power of (b) 5 and (c) 70 W, an argon carrier gas flow rate of 20 sccm, and a fixed system pressure of 100 Pa.

formation of active sites or species (radicals or ions), the recombination of the active fragments, and the coupling of the active fragments to the activated substrates to result in polymer grafting and deposition. Undesirable side reactions, such as cross-linking and substrate ablation, take place during the plasma deposition process.³¹ The atomic polymerization reaction appears to be a reasonable mechanism for plasma polymerization.³² For the application of the deposited film as an adhesion and electroless metallization promoter in microelectronics packaging, retention of the functional groups during the plasma polymerization process becomes the most important issue.

To preserve the pyridine functional groups in the pp4VP films, polymerization should be initiated through the activation of a carbon-carbon double bond. There are substantial differences in bond dissociation energy for organic molecules, viz., 267 kJ/mol for the π bond of the C=C structure, 351 kJ/mol for the C-C bond, 305 kJ/mol for the C-N bond, and 614 kJ/mol for the C=N bond.³³ The difference in bond dissociation energy gives rise to chemical structures of pp4VP that are dependent on the plasma rf power. The plausible mechanisms of activation for the 4VP monomer during the deposition of pp4VP films are illustrated schematically in Fig. 5. Under the low rf power, activation occurs mainly through the π bond of the C=C vinyl group, as the π bond has the lowest bond dissociation energy. With the increase in rf power, more active species and radicals are generated from the excitation of the C-C bond, the dissociation of the C-H bond, and the opening of the pyridine rings. The increase in the number of active species and excited states readily results in a pp4VP polymer which is structurally more complex.

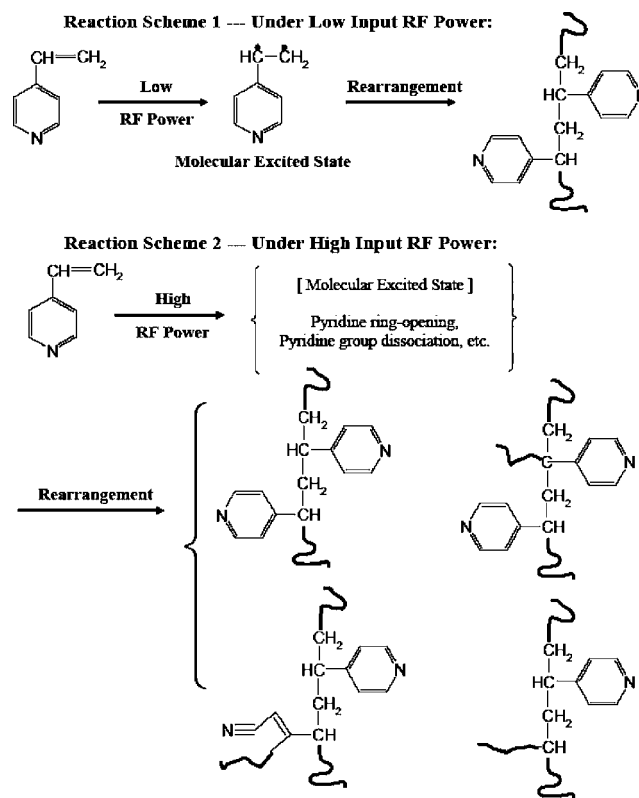


Figure 5. The plausible processes of molecular rearrangement and radical formation when 4VP is activated under low- and high-energy glow discharge conditions.

Effect of plasma parameters on the chemical composition of the Si-SiLK-g-pp4VP surface.—Figure 6 shows the wide scan and C 1s core-level spectra of the pristine SiLK surface (part a), and the Si-SiLK-g-pp4VP surfaces prepared at rf power of 5 W (part b) and 20 W (part c). The presence of grafted 4VP polymer can be deduced from the appearance of the N 1s core-level signal in the wide scan spectra of Fig. 6b and c, and the C-N peak component at the BE of 285.3 eV in the C 1s core-level spectra.

It is well known that the operating conditions, such as the type of monomer, flow rate, system pressure, and rf power, affect the nature of plasma and plasma-deposited polymer.³³ Figure 7 shows the dependence of the graft concentration of pp4VP on the input rf power, carrier gas flow rate, and system pressure. The graft concentration of the 4VP polymer on the SiLK surface is expressed, for simplicity, as the [N]/[C] ratio, because each 4VP unit contains one nitrogen atom. At a fixed chamber pressure of 100 Pa and a fixed gas flow rate of 20 sccm, the [N]/[C] ratio increases with the input rf power and reaches a maximum value of about 0.14 at the rf power of about 20 W. This [N]/[C] ratio coincides with the theoretical [N]/[C] ratio of the 4VP polymer and suggests the complete coverage of SiLK surface (to beyond the probing depth of the XPS technique) by pp4VP. Further increase in rf power simply induces the etching effect. Thus, the rf power for plasma polymerization is fixed at 20 W in this study.

Under a fixed rf power at 20 W and fixed system pressure of 100 Pa, the graft concentration increases mildly with the carrier gas flow rate up to 20 sccm, followed by a sharp decrease. Assuming that the carrier gas is saturated with the 4VP monomer, the molar flow rate of the monomer (F) increases with the increase in the Ar carrier gas flow rate. At a low carrier gas flow rate, the residence time of the monomer for plasma polymerization and the energy per unit mass of the monomer are large. The prolonged plasma state and the relatively high energy per unit mass of the 4VP molecules

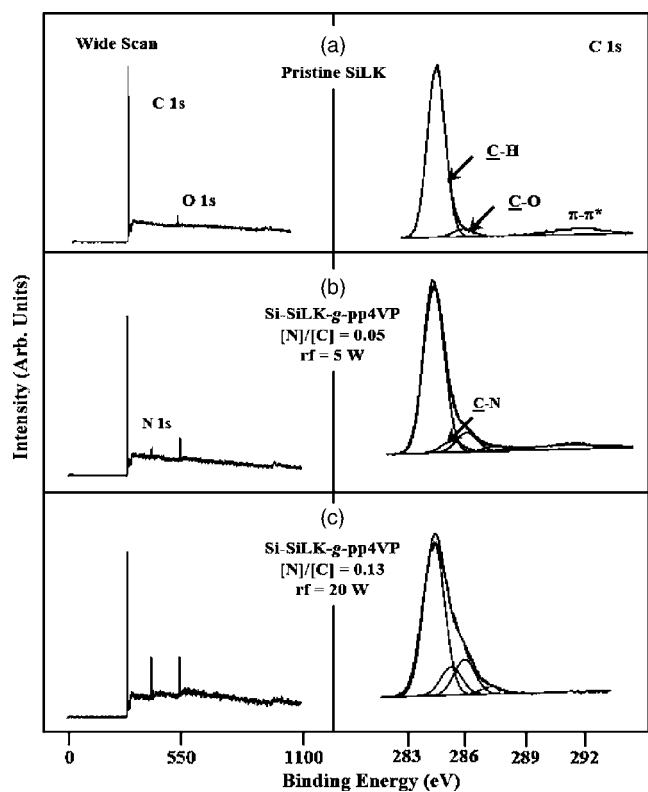


Figure 6. Wide scan and C 1s core-level spectra of the (a) pristine Si-SiLK surface, and the Si-SiLK-g-pp4VP surfaces prepared from the 5 s Ar-plasma-pretreated Si-SiLK surfaces at the input rf power of (b) 5 and (c) 20 W, an argon carrier gas flow rate of 20 sccm and a fixed system pressure of 100 Pa.

results in a high graft concentration. An increase in gas flow rate above 20 sccm reduces the residence time and energy per unit mass of the 4VP monomer molecules, resulting in a decrease in graft concentration.

Under a fixed rf power at 20 W and a fixed carrier gas flow rate at 20 sccm, the graft concentration reaches a maximum at a system pressure of 100 Pa. Further increase in system pressure leads to a reduction in graft concentration. An increase in system pressure is equivalent to an increase in the amount of 4VP monomer, and thus a decrease in energy per unit mass of the monomer, in the chamber. Hence, the optimum plasma graft polymerization condition is at a system pressure of 100 Pa, an argon carrier gas flow rate of 20 sccm, and an input rf power of 20 W. This set of plasma graft copolymerization conditions was applied to both the dense and porous SiLK for diffusion studies.

Surface morphology and electroless metallization.—Figure 8 shows the AFM images of the pristine SiLK surface (part a), the 5 s Ar-plasma-treated SiLK surface (part b), and the Si-SiLK-g-pp4VP surfaces prepared at the input rf power of 5 W (part c) and 20 W (part d). The spin-on SiLK surface is smooth and uniform, having a surface roughness (R_a) value of only 0.5 nm. The brief Ar plasma treatment resulted in only a marginal increase in surface roughness. The Si-SiLK-g-pp4VP surface prepared at the input rf power of 5 W shows an increase in surface roughness to about 1.1 nm. The R_a value increases further to about 1.9 nm for the Si-SiLK-g-pp4VP surface with a higher graft concentration and prepared at the input rf power of 20 W.

Table I shows the 180°-peel adhesion strength of copper, deposited via the two-step activation process, as well as via the SnCl₂-free one-step process, with the pristine SiLK and Si-SiLK-g-pp4VP. The adhesion strength of the electrolessly deposited copper with the pristine SiLK surface is only about 0.5 N/cm. The adhesion strength of

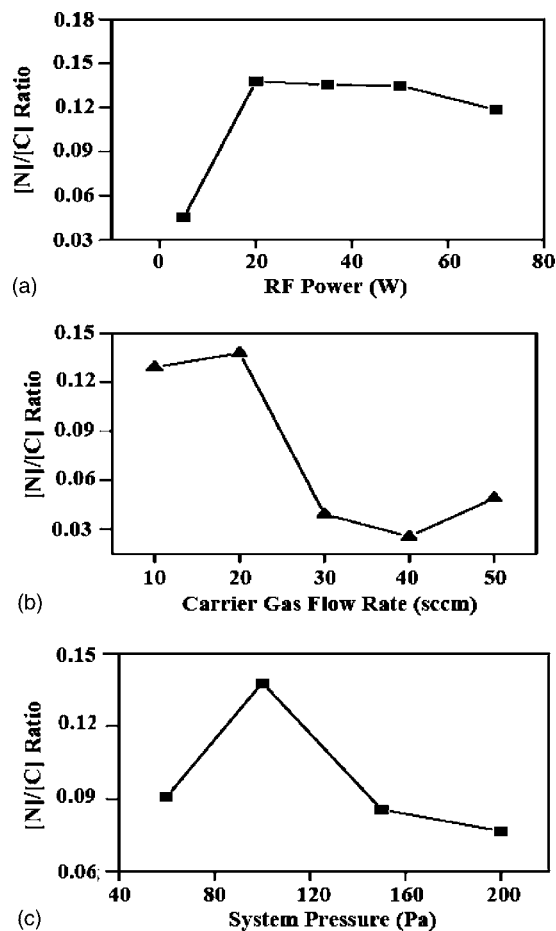


Figure 7. Effect of input rf power, carrier gas flow rate, and system pressure on the graft concentration of the pp4VP on the Si-SiLK surface.

the electrolessly deposited copper with the Si-SiLK-g-pp4VP surface is much higher (>4 N/cm). The improved adhesion strength of the electrolessly deposited copper with the Si-SiLK-g-pp4VP surface can be explained in terms of the microscopic interactions between the copper atoms and the pp4VP chains at the metal/pp4VP interface and in the metal matrix. The spatial distribution of the graft chains, and thus the pyridine rings, on the SiLK surface dictates the formation of an interphase consisting of an interpenetrating network of the graft chains in the copper matrix.³⁴ In addition to the formation of Pd-N complex during the activation step,³⁵ the nitrogen atoms from the pyridine rings of the Si-SiLK-g-pp4VP surface can also interact directly with the electrolessly deposited copper via the formation of Cu-N bonds.³⁵⁻³⁷

The adhesion failure mode of the electrolessly deposited copper with the Si-SiLK-g-pp4VP surface was studied by analyzing the chemical composition of the delaminated surfaces. Figure 9 shows the wide scan and N 1s core-level spectrum of the delaminated copper surface and the delaminated Si-SiLK-g-pp4VP surface from a Si-SiLK-g-pp4VP/Cu assembly having an adhesion strength of about 4 N/cm (sample 3, Table I). The presence of a N signal on both of the delaminated surfaces indicates that the adhesion failure occurs inside the pp4VP layer. The strong Cu signal observed in the wide scan spectrum of the delaminated copper surface indicates that the thickness of the pp4VP layer retained on the delaminated copper surface is below the probing depth of XPS technique (~ 7.5 nm in an organic matrix³⁸).

Copper diffusion studies using RBS and TEM.—Figure 10 shows the RBS spectra of the copper-metallized dense SiLK (part a) and dense SiLK-g-pp4VP (part b) surfaces on Si(100) substrates

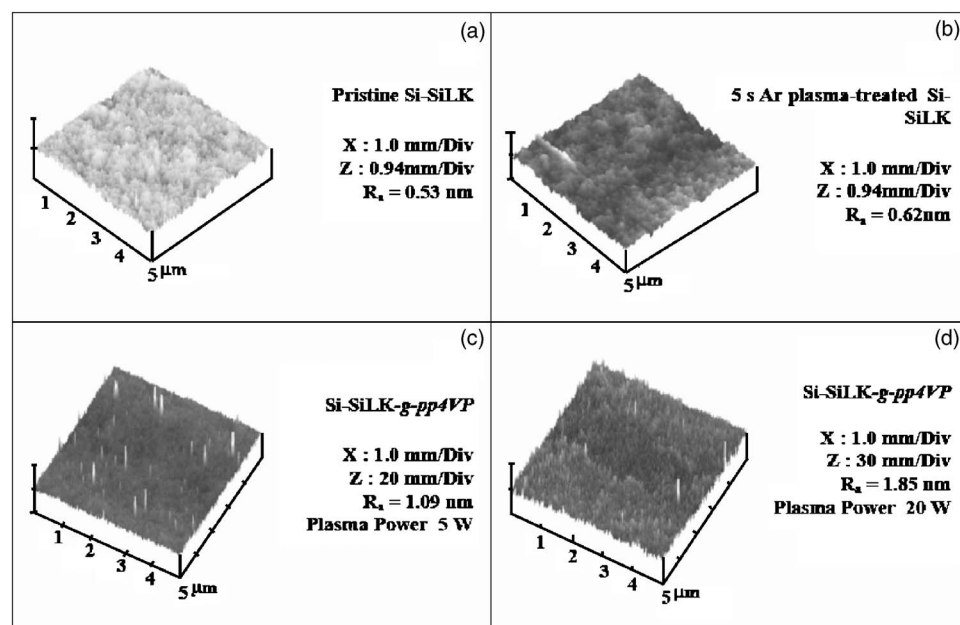


Figure 8. The surface morphology of (a) the pristine dense SiLK, (b) the corresponding 5 s Ar-plasma-pretreated SiLK, and the corresponding Si-SiLK-g-pp4VP deposited at (c) 5 and (d) 20 W, at an argon carrier gas flow rate of 20 sccm and a fixed system pressure of 100 Pa.

before and after annealing at 300°C for 5 h. As the RBS utilizes the backscattered He⁺ ion to measure the atom position and amount, a higher He⁺ ion energy indicates collision of the He⁺ ions with the heavier metal atoms, and vice versa.³⁹ Four main elements, viz., palladium, copper, silicon, and carbon, were detected in the RBS spectra. The Pd catalyst is represented by the small peak at the highest backscattered He⁺ energy, as it is the heaviest metal atoms but in smallest concentration. The carbon signal is detected at the lowest backscattered energy, as carbon is the lightest atom detectable by the RBS technique.

For the dense Si-SiLK-g-pp4VP surface in Fig. 10b, the spectrum remains practically unchanged after thermal annealing, indicating that there is no detectable copper diffusion into the dense SiLK even after annealing. For the pristine SiLK surface (Fig. 10a), the copper peak is significantly broadened on the low-energy edge side after annealing at 300°C. The carbon signal in the low-energy region has decreased substantially, as a result of intermixing of the metal with the polymer substrate. Severe diffusion of copper into SiLK can be concluded. Thus, comparison of the RBS spectra in parts (a) and (b) of Fig. 10 indicates that copper diffusion can be effectively minimized when a pp4VP layer is grafted on the dense SiLK surface.

Table I. Effect of plasma graft polymerization of 4VP on the adhesion strength of electrolessly plated copper with the Si-SiLK surface.

Surface treatment conditions		Activation method	180°-peel adhesion strength (N/cm)
Dense SiLK	1. Pristine Si-SiLK	Two-step process ^a	0.5 ± 0.1
	2. Si-SiLK-g-pp4VP ^b	Two-step process	3.5 ± 0.3
	3. Si-SiLK-g-pp4VP	Sn-free process ^c	4.0 ± 0.1
Porous SiLK	4. Si-SiLK-g-pp4VP	Two-step process	3.4 ± 0.2
	5. Si-SiLK-g-pp4VP	Sn-free process ^c	4.3 ± 0.3

^a Sensitization in SnCl₂ solution followed by surface activation in PdCl₂ solution.

^b Plasma graft polymerization of 4VP on the Ar-plasma-pretreated Si-SiLK surface, rf power 20 W, system pressure 100 Pa, carrier gas flow rate 20 sccm, [N]/[C] = 0.14.

^c Direct activation in PdCl₂ solution.

Figure 11 shows the RBS spectra of the copper-metallized porous SiLK (part a) and porous SiLK-g-pp4VP (part b) surfaces on Si(100) substrates before and after annealing at 300°C for 5 h. In Fig. 11b, the spectrum remains practically unchanged after thermal annealing at 300°C, indicating that there is no appreciable copper diffusion into the porous SiLK even after annealing. For the pristine porous SiLK surface (part a), the appearance of a diffused low-energy edge in the copper peak indicates the diffusion of copper into the porous SiLK film. Comparison of the RBS spectra in Fig. 11a and b again suggests that the surface-grafted pp4VP layer serves as an effective diffusion barrier for copper into porous SiLK. Similar results were obtained for annealing carried out at a lower temperature of 250°C but with a prolonged annealing time of 24 h.

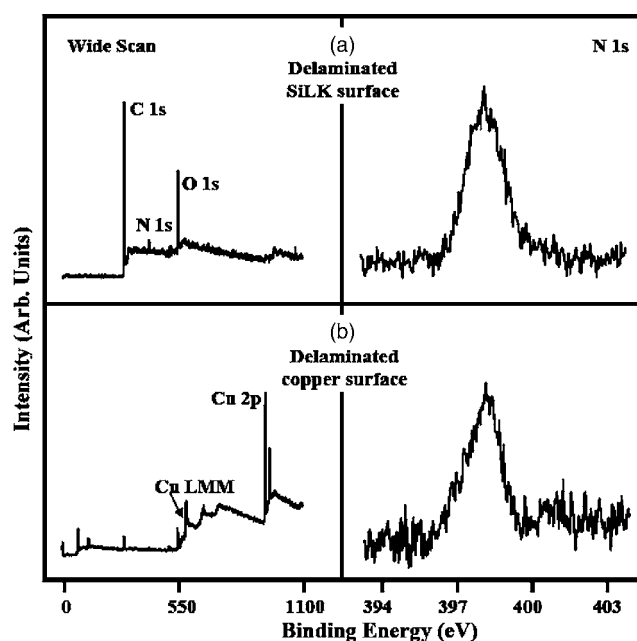


Figure 9. Wide scan and N 1s core-level spectra of (a) the delaminated Si-SiLK-g-pp4VP surface and (b) the delaminated copper surface (sample 3, Table I).

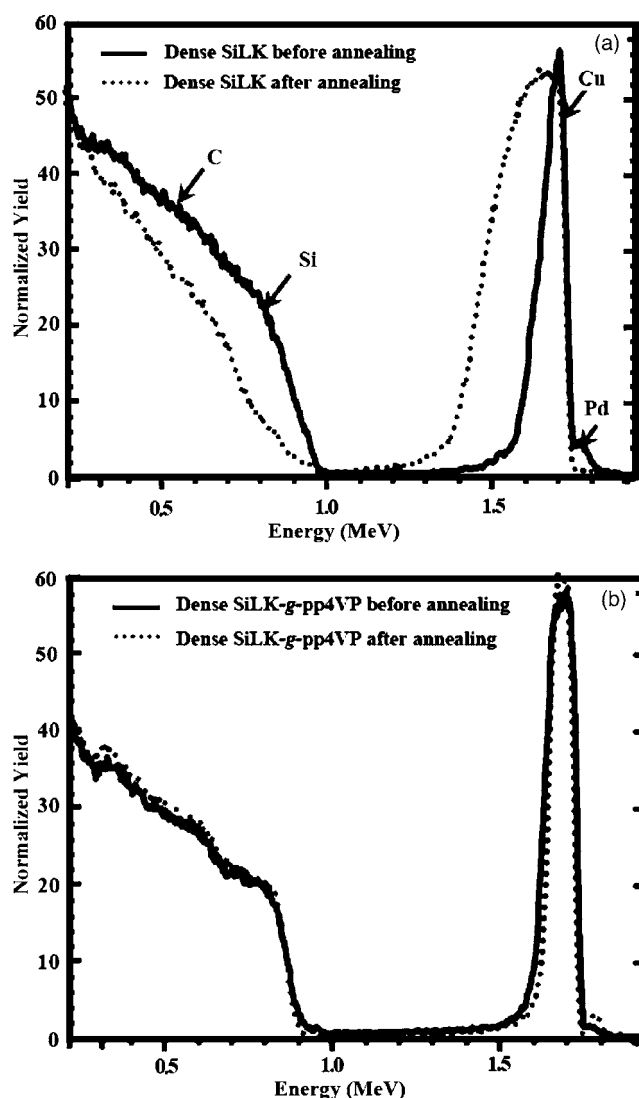


Figure 10. RBS spectra of copper diffusion in (a) the dense SiLK and (b) the dense SiLK-g-pp4VP on Si(100) with and without annealing at 300°C for 5 h.

Comparison of RBS spectra in Fig. 10a and Fig. 11a indicates that broadening of the copper peak on the lower energy side is much more significant for the dense SiLK than for the porous SiLK. The result suggests a higher extent of copper diffusion into the dense SiLK than into the porous SiLK. The reduced cross-sectional area for diffusion in the porous SiLK could lead to a lower extent of net diffusion into the porous film. Moreover, the effective path for copper diffusion across the porous film is much longer than that for copper diffusion across the dense film.⁴⁰ It has been reported that the diffusivity of copper in porous Si is seven orders of magnitude lower than that in bulk Si.⁴¹

The RBS data are further supported by the cross-sectional TEM image of the annealed (300°C, 5 h) Cu/porous SiLK interface, as shown in Fig. 12. The dark spots that are distributed on top of and inside the porous SiLK thin film are copper clusters. The formation of metal clustering is probably due to the high cohesive energy of the metal and low metal-polymer interaction energy. The clustering phenomenon agrees with that reported in the previous studies.⁴²⁻⁴⁵ The embedding of copper clusters results from the reduction in surface Gibbs free energy.⁴⁶ The size of the clusters and the embedding depth are dependent on the surface energy of the metal and polymer, as well as their interaction energy.⁸ In the case of the dense SiLK

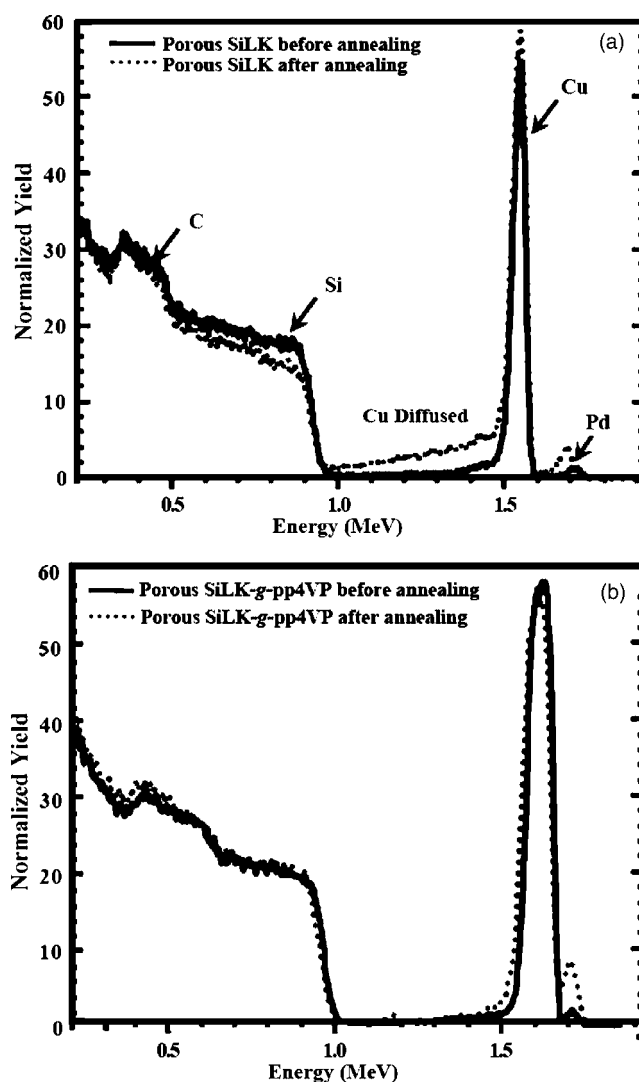


Figure 11. RBS spectra of copper diffusion in (a) the porous SiLK and (b) the porous SiLK-g-pp4VP on Si(100) with and without annealing at 300°C for 5 h.

film, no copper clusters or agglomerates were found in the near-surface region of the film after annealing under the same conditions. This phenomenon is consistent with the presence of reduced interfacial interaction energy between copper and the dense SiLK. In the presence of the surface-grafted pp4VP film, copper diffusion was significantly retarded in both dense and porous SiLK films. As a result, no copper clusters were discernible in the cross-sectional TEM images of the interfaces.

Conclusions

Plasma-induced graft polymerization of 4VP on the Ar-plasma-pretreated dense and porous SiLK surface can give rise to a thin film of covalently bonded pp4VP with retained pyridine rings. The plasma-graft-copolymerized 4VP layer can be utilized not only as the chemisorption site for the Pd complex in the Sn-free electroless copper deposition process, but also as the adhesion promotion layer for the electrolessly deposited copper. The adhesion strength of copper to the SiLK with surface-grafted pp4VP can reach above 4 N/cm. More importantly, the pp4VP graft layer acts as an effective diffusion barrier for copper into SiLK, even after annealing at 300°C for 5 h. The good adhesion strength and barrier property of the grafted pp4VP layer toward copper can be attributed to the strong interaction of the pyridine functional groups of the grafted

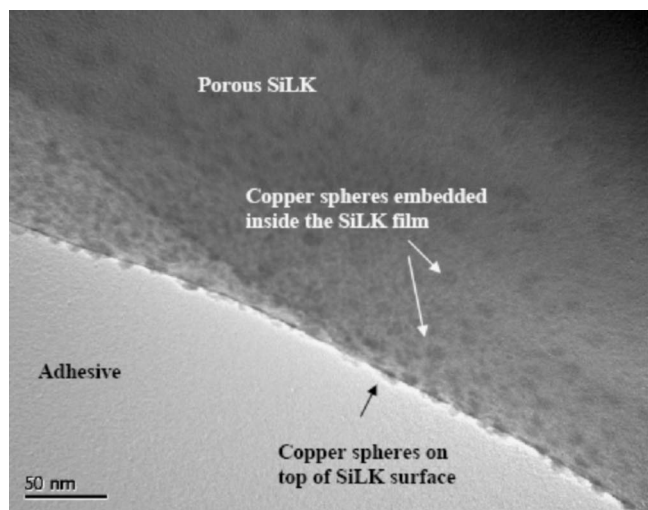


Figure 12. TEM image revealing copper diffusion into the pristine porous SiLK after thermal annealing at 300°C for 5 h.

pp4VP with palladium and copper, as well as the spatial distribution of the pp4VP chains into the electrolessly deposited metal matrix.

References

- M. Morgen, E. T. Ryan, J. H. Zhao, C. Hu, T. Cho, and P. S. Ho, *Annu. Rev. Mater. Sci.*, **30**, 645 (2000).
- P. Springer, *Semicond. Int.*, **17**, 52 (1994).
- C. Feger and H. Franke, in *Polyimides: Fundamentals and Applications*, M. K. Ghosh and K. L. Mittal, Editors, p. 759, Marcel Dekker, New York (1996).
- A. E. Dolbak, R. A. Zhachuk, and B. Z. Olshanetsky, *Semiconductors*, **35**, 1018 (2001).
- N. Aoi, *Jpn. J. Appl. Phys., Part 1*, **36**, 1355 (1997).
- K. L. Fang and B. Y. Tsui, *J. Appl. Phys.*, **93**, 5546 (2003).
- S. Q. Wang, S. Suthar, C. Hoefflichm, and B. J. Burrow, *J. Appl. Phys.*, **73**, 2301 (1993).
- F. Faupel, R. Willecke, and A. Thran, *Mater. Sci. Eng., R.*, **22**, 1 (1998).
- J. Li, Y. Shacham Diamand, and J. W. Mayer, *Mater. Sci. Rep.*, **9**, 1 (1992).
- K. Maex, M. R. Baklanov, D. Shamiryan, F. Lacopi, S. H. Brongersma, and Z. S. Yanovitskaya, *J. Appl. Phys.*, **93**, 8793 (2003).
- V. M. Dubin, Y. Shacham Diamand, B. Zhao, P. K. Vasudev, and C. H. Ting, *J. Electrochem. Soc.*, **144**, 898 (1997).
- Y. Okinaka and T. Osaka, in *Advances in Electrochemical Science and Engineering*, Vol. 3, H. Gerischer and C. W. Tobias, Editors, p. 55, VCH, Weinheim (1994).
- P. J. O'Kelly, F. K. Mongey, Y. Gobil, J. Torres, P. V. Kelly, and G. M. Crean, *Microelectron. Eng.*, **50**, 473 (2000).
- G. Muller and D. W. Baudrand, *Plating on Plastics: A Practical Handbook*, p. 80, Robert Draper, Ltd., Teddington, U.K. (1971).
- R. L. Meek, *J. Electrochem. Soc.*, **122**, 1478 (1975).
- R. L. Jackson, *J. Electrochem. Soc.*, **137**, 95 (1990).
- W. J. Dressick, C. S. Dulcey, J. H. Georger, G. S. Calabrese, and J. M. Calvert, *J. Electrochem. Soc.*, **141**, 210 (1994).
- P. H. Townsend, S. J. Martin, J. Godschalx, D. R. Romer, D. W. Smith, Jr., D. Castillo, R. DeVries, G. Buske, N. Rondan, S. Froelicher, J. Marshall, E. O. Shaffer, and J. H. Im, *Mater. Res. Soc. Symp. Proc.*, **476**, 9 (1997).
- D. A. Babb, D. W. Smith, Jr., S. J. Martin, and J. P. Godschalx (Inventors), World Patent WO 97/10193, The Dow Chemical Company (1997).
- S. J. Martin, J. P. Godschalx, M. E. Mills, E. O. Shaffer, and P. H. Townsend, *Adv. Mater. (Weinheim, Ger.)*, **12**, 1769 (2000).
- J. C. Maisonobe, G. Passemard, C. Lacour, C. Lecornec, P. Motte, P. Noël, and J. Torres, *Microelectron. Eng.*, **50**, 25 (2000).
- Z. J. Yu, E. T. Kang, and K. G. Neoh, *J. Electrochem. Soc.*, **149**, C10 (2002).
- M. C. Zhang, E. T. Kang, K. G. Neoh, and K. L. Tan, *J. Electrochem. Soc.*, **148**, C71 (2001).
- E. T. Kang and Y. Zhang, *Adv. Mater. (Weinheim, Ger.)*, **12**, 1481 (2000).
- Y. Zhang, K. L. Tan, G. H. Yang, E. T. Kang, and K. G. Neoh, *J. Electrochem. Soc.*, **148**, C574 (2001).
- G. H. Yang, E. T. Kang, and K. G. Neoh, *J. Polym. Sci., Part A: Polym. Chem.*, **38**, 3498 (2000).
- H. Ebneth, in *Metallizing of Plastics, Handbook of Theory and Practice*, R. Suchentrunk, Editor, p. 30, ASM International, Materials Park, OH (1993).
- J. F. Moulder, W. F. Stickle, P. E. Sobol, and K. D. Bomben, in *Handbook of X-Ray Photoelectron Spectroscopy*, J. Chastian, Editor, p. 40, Perkin-Elmer, Eden Prairie, MN (1992).
- H. Fochler, J. Mooney, L. Ball, R. Boyer, and J. Grasselli, *Spectrochim. Acta, Part A*, **41**, 271 (1985).
- A. S. Ellaboudy, P. J. O'Conner, and J. C. Tou, *J. Appl. Polym. Sci.*, **60**, 637 (1996).
- N. Ingaki, *Plasma Surface Modification and Plasma Polymerization*, Chap. 5, Technomic, Lancaster, PA (1996).
- C. M. Chan, T. M. Ko, and H. Hiraoka, *Surf. Sci. Rep.*, **24**, 3 (1996).
- H. Yasuda, *Plasma Polymerization*, Chap. 3, Academic Press, New York (1985).
- W. C. Wang, R. K. H. Vora, E. T. Kang, and K. G. Neoh, *Macromol. Mater. Eng.*, **288**, 152 (2003).
- G. H. Yang, E. T. Kang, K. G. Neoh, Y. Zhang, and K. L. Tan, *Langmuir*, **17**, 211 (2001).
- B. L. Rivas, H. A. Maturana, and E. Pereira, *Angew. Makromol. Chem.*, **220**, 61 (1994).
- A. M. Lyons, M. J. Vasile, E. M. Pearce, and J. V. Waszczak, *Macromolecules*, **21**, 3125 (1988).
- K. L. Tan, L. L. Woon, E. T. Kang, and K. G. Neoh, *Macromolecules*, **26**, 2832 (1993).
- Characterization in Silicon Processing*, Y. Strusser, Editor, p. 204, Butterworth-Heinemann, London (1993).
- S. Rogojevic, A. Jain, W. N. Gill, and J. L. Plawsky, *J. Electrochem. Soc.*, **149**, F122 (2002).
- D. Andsager, J. M. Hetrick, J. Hilliard, and M. H. Nayfeh, *J. Appl. Phys.*, **77**, 4399 (1995).
- C. Shim, J. Choi, D. Jung, N. E. Lee, and C. W. Yang, *Jpn. J. Appl. Phys., Part 2*, **39**, L1327 (2000).
- K. Akamatsu, T. Kawamura, H. Nabika, S. Deki, T. Strunskus, and F. J. Faupel, *Mater. Chem. Phys.*, **12**, 3610 (2002).
- T. Strunskus, M. Kiene, R. Willecke, A. Thran, C. von Bechtolsheim, and F. Faupel, *Mater. Corros.*, **49**, 180 (1998).
- V. Zaporozhtchenko, T. Strunskus, K. Behnke, C. von Bechtolsheim, M. Kiene, and F. Faupel, *J. Adhes. Sci. Technol.*, **14**, 467 (2000).
- G. J. Kovacs and P. S. Vincett, *J. Colloid Interface Sci.*, **90**, 335 (1982).